# Numerical study of three-dimensional non-Darcy forced convection in a square porous duct

G. Chen and H.A. Hadim

*Department of Mechanical Engineering, Stevens Institute of Technology Hoboken, New Jersey, USA*

***Keywords*** *Forced convection, Porous medium*

***Abstract*** *The objective of the present work was to perform a detailed numerical study of laminar forced convection in a three-dimensional square duct packed with an isotropic granular material and saturated with a Newtonian fluid. Hydrodynamic and heat transfer results are reported for three different thermal boundary conditions. The flow in the porous medium was modeled using the semi-empirical Brinkman-Forchheimer-extended Darcy model which also included the effects of variable porosity and thermal dispersion. Empirical models for variable porosity and thermal dispersion were determined based on existing three-dimensional experimental measurements. Parametric studies were then conducted to investigate the effects of particle diameter, Reynolds number, Prandtl number and thermal conductivity ratio. The results showed that channeling phenomena and thermal dispersion effects are reduced considerably in a three-dimensional duct compared with previously reported results for a two-dimensional channel. It was found that the Reynolds number affects mainly the velocity gradient in the flow channeling region, while the particle diameter affects the width of the flow channeling region. As the Reynolds number increases or as the particle diameter decreases (i.e., when the inertia and thermal dispersion effects are enhanced), the Nusselt number increases. The effects of varing the Prandtl number on the magnitude of the Nusselt number were found to be more significant than those of the thermal conductivity ratio. Finally, the effects of varing the duct aspect ratio on the friction factor can be neglected for small particle diameter ($D_p \leq 0.01$) or for high particle Reynolds number ($Re_d \geq 1000$) due to the dominant bulk damping resistance from the porous matrix (Darcy term) or strong inertia effects (Forchheimer term), respectively.*

## Nomenclature

$a$ = height of the rectangular duct
$A$ = aspect ratio = $a/b$
$b$ = width of the rectangular duct
$c$ = specific heat
$C_F$ = inertia coefficient
$C_p$ = empirical constant defined in equation (6)
$Da$ = Darcy number = $K/D_h^2$
$D_h$ = hydraulic diameter = $2ab/(a + b)$
$d_p$ = particle diameter
$D_p$ = dimensionless particle diameter = $d_p/D_h$
$D_T$ = empirical constant defined in equation (9)
$f$ = Fanning friction factor = $(dp/dx)\, D_h/(2\rho u_m^2)$
$h$ = heat transfer coefficient
$K$ = permeability of the packed bed
$k_e$ = effective thermal conductivity of the packed bed
$k_f$ = thermal conductivity of the fluid
$k_o$ = stagnant thermal conductivity of the packed bed
$k_s$ = thermal conductivity of the solid particle
$k_T$ = transverse thermal dispersion conductivity of the packed bed
$I$ = wall function, defined in equation (10)
$N$ = empirical constant defined in equation (6)
$n_d$ = inward distance normal to the wall
$N_u$ = local Nusselt number = $hD_h/k_f$
$Nu_{fd}$ = fully developed Nusselt number
$p$ = pressure
$Pe$ = Peclet number = $RePr$
$Pr$ = Prandtl number = $(\mu/\rho\alpha)_f$

International Journal of Numerical Methods for Heat & Fluid Flow, Vol. 9 No. 2, 1999, pp. 151-169,

$q'$ = heat flux per unit length of duct
$q''$ = heat flux per unit area of heating duct wall
$Re$ = Reynolds number based on hydraulic diameter = $\rho u_m D_h/\mu$
$Re_d$ = Reynolds number based on particle diameter = $\rho u_m d_p/\mu = ReD_p$
$T$ = temperature
$u$ = axial fluid velocity
$U$ = dimensionless axial fluid velocity = $u/u_m$
$x$ = axial coordinate
$X$ = dimensionless axial coordinate = $x/D_h$
$y$ = transverse coordinate along the duct height
$Y$ = dimensionless transverse coordinate = $y/D_h$
$z$ = transverse coordinate along the duct width
$Z$ = dimensionless transverse coordinate = $z/D_h$

*Greek symbols*

$\alpha$ = fluid thermal diffusivity = $k_f/(\rho c)_f$
$\varepsilon$ = porosity
$\lambda$ = thermal conductivity ratio = $k_f/k_s$
$\mu$ = dynamic viscosity of the fluid
$\rho$ = fluid density
$\omega$ = empirical constant defined in equation (10)
$\theta$ = dimensionless temperature = $(T - T_o)/(q'/k_f)$ for H1 boundary condition; $(T - T_o)/(q''D_h/k_f)$ for H2 boundary condition; $(T - T_w)/(T_o - T_w)$ for T boundary condition
$\Phi$ = transport variable

*Subscripts*

$e$ = effective (i.e. fluid-saturated porous medium)
$f$ = fluid
$m$ = mean
$o$ = inlet
$s$ = solid
$w$ = wall

## Introduction

Fundamental studies of thermal convection in porous media have increased significantly during recent years. Such a strong interest stems from the various practical applications involving porous media such as compact heat exchangers, geothermal systems, thermal insulation, energy storage units, ceramic processing, packed bed chemical reactors, and heat transfer enhancement which has received significant recent interest especially in high heat flux environments. Extensive reviews of heat transfer and flow of Newtonian fluids in porous media were provided by Nield and Bejan (1992) and Kaviany (1995).

Modeling of forced convection in porous media involves several important physical phenomena. Since the important work of Vafai and Tien (1981), a large number of studies have been reported on the boundary and inertia effects on thermal convection in porous media. Forced convective flows in variable porosity media were investigated experimentally and theoretically by Vafai (1994) and Vafai *et al.* (1985) who discussed in detail the channeling phenomena.

Thermal dispersion has been shown to be responsible for forced convection heat transfer enhancement using a porous material especially at high Reynolds number. Koch and Brady (1985) presented a dispersion model in fibrous media. Hunt and Tien (1988) conducted experiments which explicitly investigated the effects of thermal dispersion in fibrous media. Cheng *et al.* (1998) and Hsu and Cheng (1990) developed a thermal dispersion model taking into consideration the wall effect and porosity variation for packed beds. More recently, Amiri and Vafai (1994) presented a comprehensive numerical analysis of the influence of these various effects including inertia, boundary, viscosity variation and thermal dispersion.

The above brief review of the literature revealed that most of the existing studies were performed using two-dimensional configurations. Three-dimensional studies of forced convection in porous media are rather limited, yet

in several practical applications such as compact heat exchangers, three-dimensional effects are significant. Because of its practical importance, the rectangular duct has received relatively more attention than other three-dimensional geometries. Vafai *et al.* (1985), and Renken and Poulikakos (1988) conducted experimental studies using rectangular channels with aspect ratios of $A = 0.25$ and $A = 0.5$, but their numerical analyses were still performed using two-dimensional models. Kuzay *et al.* (1991) reported an experimental study of enhanced heat transfer in a metal-wool-filled square duct, and they concentrated on the high Reynolds number flow in low permeability fibrous media. Chou *et al.* (1992) conducted an experimental and numerical study of non-Darcy forced convection in a horizontal square packed-sphere channel. In their numerical model, they used empirical coefficients for variable porosity formulation which were obtained from experiments performed by Renken and Poulikakos (1988) in a rectangular duct with an aspect ratio of 0.5. Recently, Hwang and Wu (1995) reported on drag and heat transfer measurements and numerical analysis for a square packed-sphere channel, but their numerical model did not consider the effects of variable porosity.

In the present work, a detailed numerical study of three-dimensional forced convection in a square duct packed with an isotropic granular material and saturated with a Newtonian fluid was performed. A set of consistent empirical models for flow channeling and thermal dispersion were determined based on existing experimental data from the literature. A parametric study of the hydrodynamics and heat transfer in the porous duct was performed for a wide range of governing parameters including particle diameter, Reynolds number, Prandtl number and thermal conductivity ratio.

## Mathematical formulation

The physical configuration considered in the present study involves a horizontal straight square duct packed with an isotropic granular material and saturated with a Newtonian fluid as shown in Figure 1. A steady, incompressible, hydrodynamically fully developed laminar flow was assumed. The local thermodynamic equilibrium was assumed between the fluid and the

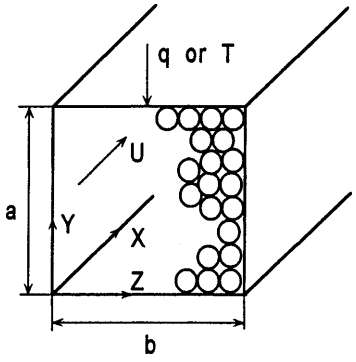


**Figure 1.**
Schematic of the physical model and coordinate system

solid matrix. The thermophysical properties of the solid matrix and of the fluid were assumed to be constant except for the variation of porosity near the walls. Natural convection and thermal radiation effects were neglected. Finally, viscous dissipation was also neglected in the energy equation.

The governing equations can then be written as (Vafai and Tien, 1981):

Continuity:

$$\frac{\partial u}{\partial x} = 0 \tag{1}$$

Momentum:

$$-\frac{\partial p}{\partial x} - \frac{\mu}{K}u - \frac{\rho C_F}{\sqrt{K}} \mid u \mid u + \frac{\mu}{\varepsilon}\left[\frac{\partial^2 u}{\partial y^2} + \frac{\partial^2 u}{\partial z^2}\right] = 0 \tag{2}$$

Energy:

$$u(y,z)\frac{\partial T}{\partial x} = \frac{1}{\rho c}\left[\frac{\partial}{\partial x}\left(k_e \frac{\partial T}{\partial x}\right) + \frac{\partial}{\partial y}\left(k_e \frac{\partial T}{\partial y}\right) + \frac{\partial}{\partial z}\left(k_e \frac{\partial T}{\partial z}\right)\right] \tag{3}$$

In the momentum equation, the permeability $K$ and the inertia coefficient $C_F$ are determined from the widely used empirical equations for flow in packed beds (Ergun, 1952):

$$K = \frac{\varepsilon^3 d_p^2}{150\,(1-\varepsilon)^2} \tag{4}$$

and

$$C_F = \frac{1.75}{\sqrt{150}\varepsilon^{\frac{3}{2}}} \tag{5}$$

The variation of porosity is approximated by the widely used exponential function of the form (Benenati and Brosilow, 1962; Chandrasekhara and Vortmeyer, 1979; Vafai, 1994):

$$\varepsilon = \varepsilon_\infty \left[1 + C_p \exp\left(-N\frac{n_d}{d_p}\right)\right] \tag{6}$$

where $\varepsilon_\infty$ is the porosity in the core region of the packed bed, and the typical value of 0.4 (Cheng *et al.*, 1988) was used in the present model. $C_p$ and $N$ are empirical constants. Due to the variation of porosity, the values of $K$ and $C_F$ vary with distance $n_d$ from the wall.

In the energy equation, the thermal dispersion conductivity in the porous matrix is accounted for as a diffusive term which is added to the stagnant thermal conductivity to get the effective thermal conductivity as (Hsu and Cheng, 1990; Hunt and Tien, 1998):

$$k_e = k_o + k_T \tag{7}$$

The stagnant thermal conductivity $k_o$ is expressed in terms of the fluid and solid thermal conductivities and the porosity using the widely accepted empirical correlation which was developed by Zehner and Schluender (1970):

$$\frac{k_o}{k_f} = 1 - \sqrt{1-\varepsilon} + \frac{2\sqrt{1-\varepsilon}}{1-\lambda B_p}\left[\frac{(1-\lambda)B_p}{(1-\lambda B_p)^2}\ln\left(\frac{1}{\lambda B_p}\right) - \frac{B_p+1}{2} - \frac{B_p-1}{1-\lambda B_p}\right] \tag{8}$$

where $B_p = 1.25\,[(1-\varepsilon)/\varepsilon]^{\frac{10}{9}}$ and $\lambda$ is the ratio of the fluid thermal conductivity to solid thermal conductivity. If the axial heat conduction effects are negligible, which is usually true for nearly parallel flows with $Re_d Pr > 1$ (Cheng *et al.*, 1988), only the transverse component of thermal dispersion conductivity is included and it is given by (Cheng *et al.*, 1988).

$$\frac{k_T}{k_f} = D_T Re_d Pr l \left(\frac{u}{u_m}\right) \tag{9}$$

where $D_T$ is an empirical constant and $l$ is a dimensionless dispersive length which accounts for the wall effect on the reduction of the lateral mixing of the fluid. A widely accepted model for the dispersive length is obtained using a Van Driest type wall function (Cheng *et al.*, 1988):

$$l = 1 - \exp\left(-\frac{n_d}{\omega d_p}\right) \tag{10}$$

where $D_T$ and $\omega$ are empirical constants which are determined in conjunction with the coefficients $C_p$ and $N$ used in the porosity variation model. The values for such a set of empirical constants have been determined for two-dimensional configurations by Cheng *et al.* (1988). However, Chou *et al.* (1992) showed that these values failed to model accurately three-dimensional rectangular ducts. Consequently, a consistent set of empirical coefficients for modeling thermal dispersion and porosity variation in a square duct should be used in the numerical model.

The mathematical formulation discussed above is based on the use of the volume averaging technique to derive the macroscopic governing equations for transport in porous media combined with appropriate empirical models including the correlations for permeability, inertia coefficient and porosity variation in the momentum equation, and for the stagnant thermal conductivity and thermal dispersion conductivity in the energy equation. Such a volume averaging technique combined with empirical correlations has been used extensively in the past and has led to the derivation of the well-established Brinkman-Forchheimer-extended Darcy model, which is the most widely accepted semi-empirical model and has provided satisfactory results for two-dimensional configurations as reported by several previous investigators

(Amiri and Vafai, 1994; Cheng *et al.*, 1998; Hsu and Cheng, 1990; Hunt and Tien, 1988; Kaviany, 1995; Vafai, 1994; Vafai and Tien, 1981). A more rigorous use of the volume averaging technique for modeling transport in porous media would lead to a large number of unknowns which would require experimental verification just as with the semi-empirical treatments (Kaviany, 1995). This is due to the complexity of the local fluid dynamics and heat transfer interactions between the fluid and the solid matrix. Therefore, although the volume averaging technique involves integration of the conservation equations over a representative elementary volume, empiricism to various extents must be applied to develop the macroscopic volume-averaged conservation equations.

As a result, a more rigorous derivation of the macroscopic equations for transport in porous media especially in three-dimensional configurations such as rectangular ducts is still an open question. In the present study, the semi-empirical Brinkman-Forchheimer-extended Darcy model is used for modeling three-dimensional forced convection in porous media, and appropriate empirical data for three-dimensional rectangular ducts are used to enhance the model and generate satisfactory results for flow and heat transfer as discussed later.

Eqs. (1-3) were converted into dimensionless form as follows:

Continuity

$$\frac{\partial U}{\partial X} = 0 \tag{11}$$

Momentum

$$2fRe - \frac{1}{Da}U - \frac{C_F Re}{\sqrt{Da}} \mid U \mid U + \frac{1}{\varepsilon}\left[\frac{\partial^2 U}{\partial Y^2} + \frac{\partial^2 U}{\partial Z^2}\right] = 0 \tag{12}$$

Energy

$$U\frac{\partial \theta}{\partial X} = \frac{1}{Pe}\left[\frac{\partial}{\partial Y}\left(\frac{k_e}{k_f}\frac{\partial \theta}{\partial Y}\right) + \frac{\partial}{\partial Z}\left(\frac{k_e}{k_f}\frac{\partial \theta}{\partial Z}\right)\right] \tag{13}$$

The velocity and thermal boundary conditions are given in dimensionless form as follows. No-slip condition is applied along the walls of the duct for the axial velocity such that

$$U(0, Z) = 0 \qquad \text{and} \qquad U(Y, 0) = 0 \tag{14}$$

A uniform temperature is assumed at the duct inlet and three types of thermal boundary conditions at the walls of the rectangular duct were considered (Irvine, 1963) as follows.

*H1 condition (constant axial wall heat flux and constant peripheral wall temperature, i.e., the wall heat flux is independent of longitudinal direction X, and the wall temperature is independent of transverse directions Y and Z):*

$$\theta(0, Y, Z) = 0 \tag{15}$$

$$\int_0^1 \left[\frac{k_o}{k_f}\frac{\partial\theta}{\partial Y}\right]_{|Z=0,1} dZ + \int_0^1 \left[\frac{k_o}{k_f}\frac{\partial\theta}{\partial Z}\right]_{|Y=0,1} dY = 1.0 \tag{16}$$

*H2 condition (constant axial and peripheral wall heat flux, i.e., the wall heat flux is independent of longitudinal direction X and transverse directions Y and Z):*

$$\theta(0,Y,Z) = 0 \tag{17}$$

$$\frac{k_o}{k_f}\frac{\partial\theta}{\partial Y}(X,Y,0) = -1.0 \text{ and } \frac{k_o}{k_f}\frac{\partial\theta}{\partial Y}(X,Y,1) = 1.0 \tag{18}$$

$$\frac{k_o}{k_f}\frac{\partial\theta}{\partial Z}(X,0,Z) = -1.0 \text{ and } \frac{k_o}{k_f}\frac{\partial\theta}{\partial Z}(X,1,Z) = 1.0 \tag{19}$$

*T condition (constant axial and peripheral wall temperature, i.e., the wall temperature is independent of longitudinal direction X and transverse directionsY and Z):*

$$\theta(0,Y,Z) = 1.0 \tag{20}$$

$$\theta(X,0,Z) = \theta(X,1,Z) = \theta(X,Y,0) = \theta(X,Y,1) = 0 \tag{21}$$

At the exit, the thermally fully developed conditions are used as (Shah and London, 1978):

$$\frac{\partial^2\theta}{\partial X^2} = 0 \text{ (H1, H2 boundary conditions);}$$

$$\frac{\partial\theta}{\partial X} = 0 \text{ (T boundary condition)} \tag{22}$$

The local dimensionless pressure drop in the momentum equation is calculated in terms of the Fanning friction factor which is defined as:

$$f = \left(-\frac{dp}{dx}\right)\frac{D_h}{2\rho u_m^2} \tag{23}$$

and the local Nusselt number is defined as:

$$Nu = \frac{k_o}{k_f}\frac{D_h}{(T_m - T_{w,m})}\left(\frac{\partial T}{\partial n_d}\right)_{w,m} \tag{24}$$

**Numerical procedure**

Numerical solutions of the governing equations (11)-(13) with the associated boundary conditions (14)-(22) were obtained using the control volume procedure outlined by Patankar (1980). After a staggered grid was arranged for the discretization process, a second-order upwind scheme was used to model the

interactions between the convection and diffusion terms in the governing equations. Darcy and Forchheimer terms in the momentum equation were treated as source terms. There are many expressions for the linearization of source terms. In the present study, the form recommended by Patankar (1980) was applied. Thus, the linearized forms of the governing equations can be summarized as

$$C_P\Phi_P = C_D\Phi_D + C_U\Phi_U + C_N\Phi_N + C_S\Phi_S + C_E\Phi_E + C_W\Phi_W + S_P^{\Phi} \quad (25)$$

Where $\Phi$ stands for the transport variables: $U$ for the momentum equation and $\theta$ for the energy equation; $C$ are coefficients combining convection terms, diffusion terms and the nonconstant parts of the linearized Darcy and Forchheimer terms; and $S$ is the sum of all source terms including pressure drop ($f\,Re$), the constant parts of linearized Darcy and Forchheimer terms, and the additional parts from the convection term due to using of second-order upwind scheme. The subscripts on $C$ denote the main grid point labeled as $P$ surrounded by the six neighboring points labeled as $D$ (downstream), $U$ (upstream), $N$ (north), $S$ (south), $W$ (west) and $E$ (east). The expressions for these coefficients are presented in Table I.

In Table I, $U^*$ denotes the guessed velocity or the previous-iteration velocity, and $b$ is the additional part from the convection term in the energy equation, these are presented in Table II.

An iterative procedure based on the SIMPLE algorithm was adopted for the momentum equations to link the pressure drop $f\,Re$ and the velocity profile $U$, while the temperature field $\theta$ was computed subsequently from the energy equation. The integral form of the continuity equation was used to correct values of the pressure drop $f\,Re$ during the iterative process. A matrix solver based on the Tri-Diagonal Matrix Algorithm (TDMA) was applied to solve the resulting discretized algebraic equations. To yield more rapid convergence, relaxation parameters were used for the velocity, pressure and temperature. Convergence from the iterative procedure was monitored by examining how well the discretization equations were satisfied by the current values of the dependent variables. The convergence criteria required that at any given grid point, the absolute value of the residual be less than $10^{-6}$. Furthermore, energy balance was preserved to within 2.0 per cent in all calculations.

The number and distribution of grids required in order to obtain acceptable accuracy were found by trial and error. For forced convection in porous media, it has been shown that solutions of the governing equations exhibit steep velocity gradients near the impermeable walls due to imposing no-slip conditions at solid surfaces, and these gradients vary with the Darcy number, particle diameter, Reynolds number and Prandtl number (Cheng *et al.,* 1988; Hunt and Tien, 1988). Furthermore, this behavior is more pronounced in the presence of channeling due to variable porosity. Consequently, a skewed grid distribution is used along all the coordinate axes such that the node density is higher in the vicinity of the walls in the transverse direction and at the entrance in the longitudinal direction. In general, it was found that a duct cross section

| Coefficient | Expression for $U$ | Expression for $\theta$ |
|---|---|---|
| $C_D$ | $0$ | $\max[-U_d \Delta Y \Delta Z,\ 0]$ |
| $C_U$ | $0$ | $\max[U_u \Delta Y \Delta Z,\ 0]$ |
| $C_N$ | $\left(\frac{1}{\varepsilon}\right)_n \frac{\Delta Z \Delta X}{\delta Y_n}$ | $\left(\frac{k_e}{k_f}\frac{1}{Pe}\right)_n \frac{\Delta Z \Delta X}{\delta Y_n}$ |
| $C_S$ | $\left(\frac{1}{\varepsilon}\right)_s \frac{\Delta Z \Delta X}{\delta Y_s}$ | $\left(\frac{k_e}{k_f}\frac{1}{Pe}\right)_s \frac{\Delta Z \Delta X}{\delta Y_s}$ |
| $C_E$ | $\left(\frac{1}{\varepsilon}\right)_e \frac{\Delta X \Delta Y}{\delta Z_e}$ | $\left(\frac{k_e}{k_f}\frac{1}{Pe}\right)_e \frac{\Delta X \Delta Y}{\delta Z_e}$ |
| $C_W$ | $\left(\frac{1}{\varepsilon}\right)_w \frac{\Delta X \Delta Y}{\delta Z_w}$ | $\left(\frac{k_e}{k_f}\frac{1}{Pe}\right)_w \frac{\Delta X \Delta Y}{\delta Z_w}$ |
| $S_P^{\Phi}$ | $\left(2fRe + \frac{C_F Re}{\sqrt{Da}}(U^*)^2\right)_P \Delta X \Delta Y \Delta Z$ | $\frac{1}{2}(b_d + b_u)$ |
| $C_P$ | $\Sigma C_{U-W} + \left(\frac{1}{Da} + 2\frac{C_F Re}{\sqrt{Da}}U^*\right)_P \Delta X \Delta Y \Delta Z$ | $\Sigma C_{U-W}$ |

**Table I.**
Coefficients of the linearization forms of governing equations

| | |
|---|---|
| $b_d$ | $\frac{\delta X_d}{\delta X_u}(U_U - U_P)\max[U_d \Delta Y \Delta Z, 0] + \frac{\delta X_d}{\delta X_{dd}}(U_D - U_{DD})\max[-U_d \Delta Y \Delta Z,\ 0]$ |
| $b_u$ | $\frac{\delta X_u}{\delta X_{uu}}(U_U - U_{UU})\max[U_u \Delta Y \Delta Z, 0] + \frac{\delta X_u}{\delta X_d}(U_D - U_P)\max[-U_u \Delta Y \Delta Z,\ 0]$ |

**Table II.**
Expressions of the additional linearization terms in the energy equation

with a $61 \times 61$ grid yielded results with less than 2 per cent error from those obtained using an $81 \times 81$ grid, and the grid number for the longitudinal direction was adjusted based on the developing length. Because this problem is strongly parabolic, the computational domain was systematically extended in the axial direction beyond the physical domain until the effects of exit boundary conditions on the flow and heat transfer in the entrance region were negligible. This was also determined based on the governing physical parameters including particle diameter, Reynolds number and Prandtl number.

## Results and discussion

In order to examine the validity and accuracy of the present numerical model, the numerical results were compared with corresponding results reported in the literature for various cases. For the case of fully developed forced convection of a Newtonian fluid in nonporous rectangular ducts with various aspect ratios

(0.0 – 1.0) and three typical thermal boundary conditions (H1, H2 and T), the results for friction factor and fully developed Nusselt number obtained in the present study were compared with the analytical, numerical and experimental results presented by Shah and London (1978). For a two-dimensional packed-sphere channel, a comparison was performed between the fully developed Nusselt number values obtained from the present model (with a duct aspect ratio, $A = 0.01$) and the corresponding results for a parallel plate channel reported by Cheng *et al.* (1988) as illustrated in Table III. Very good agreement was found in all cases.

To determine consistent empirical models for the porosity variation and thermal dispersion for a three-dimensional rectangular duct, the experimental measurements reported by Hwang and Wu (1995), and by Chou *et al.* (1992) were used. The experimental measurements of Hwang and Wu (1995) were conducted using a square channel filled with packed spheres. In order to determine permeability and inertia coefficient graphically, they showed that the pressure drop was proportional to the particle Reynolds number because their data were located in the Forchheimer flow regime due to the high particle Reynolds number used ($200 < Re_d < 2000$). However, the porosity variation near the wall was neglected in their numerical analysis. Based on previous two-dimensional studies of packed-sphere channels, the porosity variation near the walls induces a channeling phenomenon which affects significantly the velocity profiles and the heat transfer (Amiri and Vafai, 1994; Cheng *et al.*, 1988; Poulikakos and Renken, 1987). In the present study, the porosity variation model was determined iteratively by varying the values of $C_p$ and $N$ until the numerical results from the present model matched the experimental data reported by Hwang and Wu (1995). For the closest agreement with experimental data as illustrated in Figure 2, the coefficients $C_p$ and $N$ for the porosity function were found to be $0.80 \pm 0.01$ and $2.0 \pm 0.1$, respectively. These values of the coefficients were then used throughout the present computations. It is noteworthy that these values of the coefficients are less than those for a parallel plate channel, i.e., $C_p = 1.4$ and $N = 5.0$ as reported by Nield and Bejan (1992) and Cheng *et al.* (1998). This indicates that some attenuation of the porosity variation near the walls exists in three-dimensional ducts compared with two-dimensional channels. The effect of the particle diameter on these coefficients was found to be negligible as shown also by Vafai (1994) for two-dimensional channels.

**Table III.**
Comparison of fully developed Nusselt number $Nu_{fd}$ results between the present study ($A$=0.01) and Cheng *et al.* (1988) ($A$=0.0)

| $D_p$ | $Re_d$ | Cheng *et al.* (1988) ($A = 0.0$) | Present work ($A = 0.01$) |
|---|---|---|---|
| 0.0185 | 97 | 243 | 240 |
| 0.0185 | 405 | 952 | 935 |
| 0.0925 | 321 | 305 | 300 |
| 0.0925 | 2248 | 1683 | 1658 |

Following the evaluation of the coefficients for porosity variation, the coefficients for the thermal dispersion model were obtained by comparing the results from the present numerical model with the experimental data reported by Chou *et al.* (1992) for a square channel filled with packed spheres. In their experiments, Chou *et al.* (1992) used ducts made of highly conductive materials such that the H1 thermal boundary condition was appropriately used in the present numerical model for comparison. In their numerical study, Chou *et al.* (1992) used empirical coefficients for the porosity variation which were inconsistent since they were based on the measurements reported by Renken and Poulikakos (1988) for a rectangular duct with aspect ratio 0.5. For the sake of gaining a set of consistent coefficients for a packed-sphere square duct, the coefficients for the transverse thermal dispersion model were determined in the present study using the more consistent coefficients for the porosity variation as determined earlier and by comparing the fully developed Nusselt number results obtained in the present study with the experimental data reported by Chou *et al.* (1992). As indicated in Figure 3, very good agreement was obtained when the coefficients $D_T$ and $\omega$ were set equal to 0.012 ± 0.002 and 2.0 ± 0.1, respectively. Similar to the coefficients for the

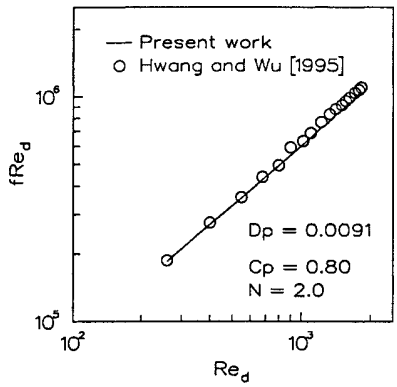


**Figure 2.**
Comparison of results for friction factor with the experimental data reported by Hwang and Wu (1995)

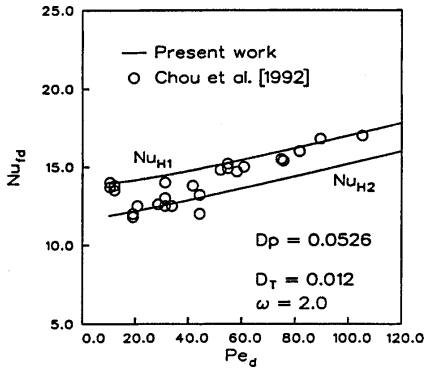


**Figure 3.**
Comparison of results for fully developed Nusselt number with the experimental data reported by Chou *et al.* (1992)

variable porosity model, the values of coefficients for the thermal dispersion model also showed that some reduction of the thermal dispersion effects occurs in three-dimensional ducts compared with two-dimensional channels. Thermal dispersion is a local mechanism which includes the wall effect due to the variable porosity and the magnitude of the local velocity. In three-dimensional ducts, the attenuation of the porosity variation near the walls leads to a decrease in peak velocity and a smaller velocity gradient within the channeling region near the walls where larger thermal dispersion effects occur. Therefore, some reduction of the thermal dispersion effects in three-dimensional ducts would then be expected.

Once the empirical models for porosity variation and thermal dispersion were determined, a parametric study was then carried out to analyze the effects of particle diameter, Reynolds number, Prandtl number and thermal conductivity ratio on velocity profiles, temperature fields, local and fully developed Nusselt numbers and pressure drop. Each of these parameters was varied over a wide range based on fundamental as well as practical considerations.

In Tables IV and V, typical values of the thermophysical properties of the porous materials and Newtonian fluids considered in the present analysis are illustrated.

### *Velocity profiles*

The effects of particle diameter and particle Reynolds number on the fully developed velocity profile are shown in Figure 4. The velocity profile is symmetric about the horizontal central axes $Y = 0.5$ and $Z = 0.5$, so only the velocity profile about $Z = 0.5$ is discussed here. It is shown that due to channeling effects, there is a large velocity gradient near the walls where the maximum velocity occurs and a flat velocity profile in the core region where the maximum velocity occurs at the center. As the particle Reynolds number increases, the velocity gradient near the wall increases but the peak velocity

**Table IV.**
Properties of selected fluids

| Liquid | $k_f$ (W/m – K) | Pr |
|---|---|---|
| Oil | 0.136 | 100 |
| Ethylene-glycol | 0.259 | 51 |
| Water | 0.616 | 7 |

**Table V.**
Thermal conductivity of selected solids

| Solid | $k_s$ (W/m – K) |
|---|---|
| Acrylic | 0.16 |
| Glass | 1.10 |
| Steel | 37.39 |

decreases. The region near the wall affected by the channeling phenomenon gets slightly narrower with increasing Reynolds number. As the particle diameter increases, the permeability of the packed bed increases which leads to increased local velocity such that the size of the channeling region increases significantly as shown in Figure 4. As the particle diameter increases, the velocity gradient near the wall decreases such that the peak velocity decreases and moves a significant distance away from the wall. Thus, the effect of Reynolds number is related to the strength of the channeling phenomenon (e.g., magnitude of the local velocity), while the effect of particle diameter is connected mostly with the width of the flow channeling region. Although these observations are consistent with those of the two-dimensional channel, important differences exist due to the attenuation of the porosity variation that occurs in three-dimensional ducts. For example, it was found that in the three-dimensional square duct, the maximum velocity occurs at a distance away from the wall of $0.11D_p$ for $Re_d = 100$ and $0.18D_p$ for $Re_d = 10$. In the two-dimensional channel, the corresponding values were $0.10D_p$ for $Re_d = 100$ and $0.15D_p$ for $Re_d = 10$. Also the peak velocity values decreased by 13 per cent to 30 per cent from the corresponding values for the two-dimensional case.

*Temperature fields*

Similar to the velocity profile, the temperature field is also symmetric about the horizontal central axes $Y = 0.5$ and $Z = 0.5$. The fully developed temperature profiles at $Z = 0.5$ are displayed in Figure 5 for the three thermal boundary conditions H1, H2 and T which were described earlier. The physical mechanisms responsible for the differences in the developing length due to different thermal boundary conditions were described in detail by Shah and London (1978) for the three-dimensional nonporous duct. In order to examine the effects of thermal dispersion on the temperature fields, both cases with thermal dispersion effects ($D_T = 0.012$) and without thermal dispersion effects ($D_T = 0.0$) were compared as shown in Figure 5. Obviously, the thermal dispersion effects increase thermal mixing which makes the temperature field

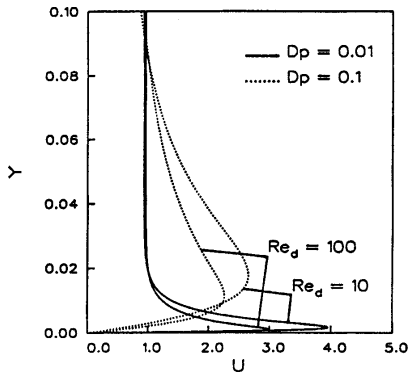


**Figure 4.**
Effects of particle diameter and Reynolds number on the axial velocity profile at $Z$=0.5

more uniform. Among the three heating conditions, the thermal dispersion effects on the temperature field for T boundary condition are most significant, and those for H1 boundary condition are least significant. When thermal dispersion effects are included, the temperature field for T boundary condition is much more uniform while the H2 condition exhibits a significant temperature gradient across the cross section. Consequently, the developing length for the T boundary condition is the shortest, while the corresponding one for the H2 boundary condition is the longest. This behavior is consistent with that of the corresponding two-dimensional case.

*Nusselt number results*

The local Nusselt number variations for the *H*1, *H*2 and *T* boundary conditions are shown in Figure 6 for $D_p$ = 0.001. The Nusselt number undergoes a large decrease in the entrance region and reaches an asymptotic limit in the fully developed region. It is shown that the difference in Nusselt number between the *T* and *H* boundary conditions is significant while that between *H*1 and *H*2 is relatively small. These differences decrease as the fully developed condition

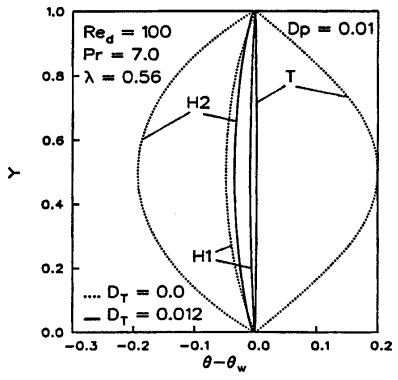


**Figure 5.**
Temperature field at $Z$ = 0.5 for H1, H2 and T boundary conditions

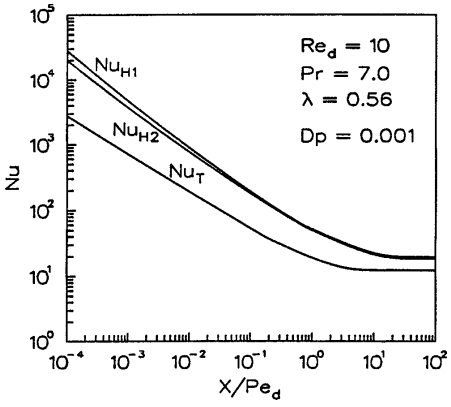


**Figure 6.**
Local Nusselt number variation for H1, H2 and T boundary conditions

is reached. As discussed earlier for the temperature fields, the variation of the thermal entrance length for the three thermal boundary conditions is confirmed in Figure 6.

The variations of the fully developed Nusselt numbers $Nu_{H1}$, $Nu_{H2}$ and $Nu_T$ with particle Reynolds number are presented in Figure 7 for the H1, H2 and T boundary conditions, respectively. It is observed that the Nusselt number $Nu_{H1}$ is always higher than $Nu_{H2}$ and $Nu_T$, which is also consistent with the results reported by Shah and London (1978) for a nonporous square duct. As expected, a high particle Reynolds number $Re_d$ generates strong convection effects and high thermal mixing, which results in a higher Nusselt number. For low $Re_d$ ($Re_d < 10$), the three fully developed Nusselt number curves remain almost constant since thermal diffusion effects are dominant while thermal dispersion effects are weak. For the two-dimensional parallel plate channel case, Cheng *et al.* (1988) showed that the thermal dispersion effects would be negligible when the particle Reynolds number $Re_d$ was less than approximately 0.1. But in the present three-dimensional case, it is shown that these effects become important for a higher value of $Re_d$, i.e., $Re_d \geq 10$. Such a behavior demonstrates that the thermal dispersion effects are reduced in the three-dimensional square duct as discussed earlier.

The combined effects of particle diameter, Prandtl number and thermal conductivity ratio on the fully developed Nusselt number are illustrated in Figure 8. Generally, the variations of the three Nusselt numbers are very similar, so only $Nu_{H1}$ as an example is discussed. Six cases representing a wide range of practical fluid and porous medium thermophysical properties as listed in Table VI were investigated.

The results for these six cases are illustrated in Figure 8 where it is shown that the Prandtl number is the dominant factor which affects more significantly the magnitude of the Nusselt number. As the Prandtl number increases, the thermal boundary layer becomes thinner and thermal dispersion effects are stronger, which leads to a significant increase in the Nusselt number. For a given Prandtl number, a smaller thermal conductivity ratio $\lambda$ results in a higher

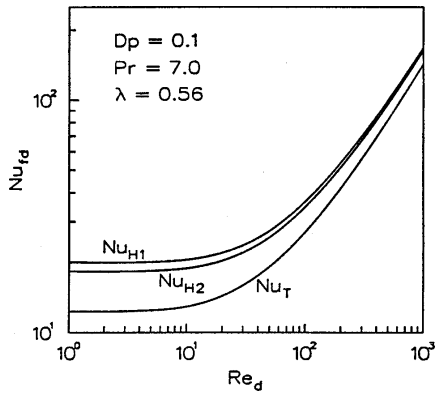


**Figure 7.**
Effects of Reynolds number on the fully developed Nusselt number variation for H1, H2, and T boundary conditions

Nusselt number. Porous media with higher thermal conductivity ratio generate higher thermal dispersion effects on heat transfer. Recently, the potential of high thermal conductivity porous media for forced convection heat transfer enhancement has received significant attention (Bartlett and Viskanta, 1996; Hwang and Chao, 1994). It is shown also in Figure 8 that the effects of thermal conductivity ratio are more significant in porous media with larger particle diameters. As the particle diameter $D_p$ decreases, the fully developed Nusselt number gradually increases and approaches an asymptotic value for low $D_p$ (e.g. Darcy regime). The limit value of $D_p$ for Darcy regime depends on $Pr$ and $\lambda$.

To analyze the effects of aspect ratio on the fully developed Nusselt number in the duct, a comparison of the results obtained for the square duct ($A$ = 1.0) and the parallel plate channel ($A$ = 0.0) is presented in Figure 9. Physically, the aspect ratios $A$ = 1.0 and $A$ = 0.0 represent the lower limit and upper limit respectively for heat transfer in rectangular ducts. Relatively, the effects of particle diameter $D_p$ on the fully developed Nusselt number for $A$ = 0.0 are more significant than those for $A$ = 1.0 beyond the Darcy regime. As $D_p$ increases, the difference between the fully developed Nusselt number for the constant wall temperature condition and the corresponding one for the constant wall heat flux condition remains relatively constant for $A$ = 1.0, but becomes smaller for $A$ = 0.0.

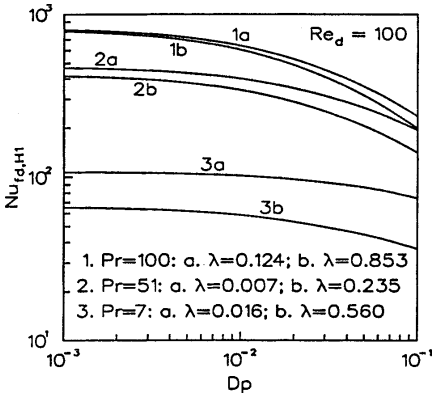


**Figure 8.**
Effects of thermal conductivity ratio and Prandtl number on the fully developed Nusselt number variation with particle diameter

| Case | Liquid | Soild | $\lambda = k_f / k_s$ |
|---|---|---|---|
| 1a | Oil | Glass | 0.124 |
| 1b | Oil | Acrylic | 0.853 |
| 2a | Ethylene-glycol | Steel | 0.007 |
| 2b | Ethylene-glycol | Glass | 0.235 |
| 3a | Water | Steel | 0.016 |
| 3b | Water | Glass | 0.560 |

**Table VI.**
Cases for the parametric studies

*Pressure drop calculations*

For engineering applications of the present study such as compact heat exchangers, it is important to know the magnitude of pressure drop caused by the presence of the porous medium in the duct. The variation of the fully developed friction factor with particle Reynolds number $Re_d$ and with particle diameter $D_p$ as a parameter is illustrated in Figure 10. The friction factor $fRe_d$ increases as $Re_d$ increases or as $D_p$ decreases as shown also by Cheng *et al.* (1988) for the parallel plate channel. A comparison of the friction factor for the square duct and for the parallel plate channel is also illustrated in Figure 10. A negligible difference between these two cases is observed for small $D_p$. The question arises as to why both curves for $A = 1.0$ and $A = 0.0$ are almost coincidental, which can be answered by examining the Forchheimer flow model.

For small $D_p$, most of the duct cross section is at the core porosity $\varepsilon_\infty = 0.4$, and the variable porosity effects are limited to a very narrow region close to the walls. The Darcy number $Da$ based on $\varepsilon_\infty$ can be evaluated by the Ergun model

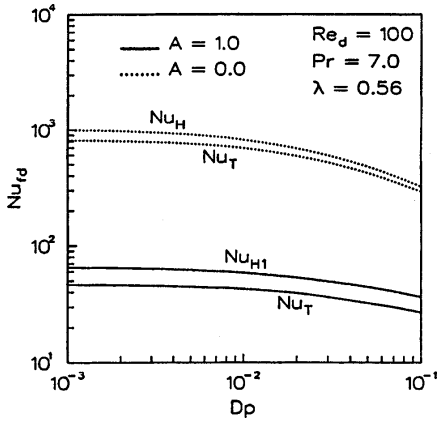


**Figure 9.**
Comparison of the fully developed Nusselt number between the square duct ($A = 1.0$) and the parallel plate channel ($A = 0.0$)

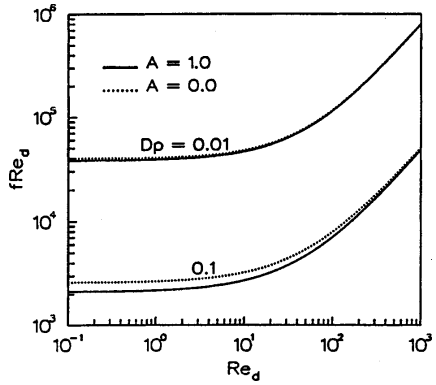


**Figure 10.**
Comparison of the friction factor with particle diameter and Reynolds number between the square duct (A = 1.0) and the parallel plate channel (A = 0.0)

for the permeability. When $D_p = 0.01$, $Da = 1.19 \times 10^{-7}$. At such a very low $Da$ value, the Brinkman term is indeed insignificant relative to the Darcy and Forchheimer terms in the momentum equation, which means that both the bulk damping resistance due to the porous structure and the resistance due to the inertia forces are much stronger than the viscous resistance at the boundary. Consequently, the dimensionless form of the Forchheimer flow model is used to approximately model the flow in the duct as:

$$2fRe_d = \frac{D_p}{Da}U + \frac{C_F Re_d}{\sqrt{Da}} \mid U \mid U \tag{26}$$

where $U$ equals 1 (for slug flow) for all $A$. Evidently, the fully developed friction factor is only dependent on the particle Reynolds number when $D_p$ and $C_F$ are specified. Finally, it is important to point out that the coincidence of both $fRe_d$ curves does not mean the same real physical and dimensional pressure drops due to different values of the corresponding hydraulic diameter for each case.

## Conclusions

A numerical study of three-dimensional non-Darcy forced convection in a square duct packed with spherical particles and saturated with a Newtonian fluid was conducted. The present model was based on a consistent set of empirical coefficients for the porosity variation and the thermal dispersion models which were determined from existing experimental data for a three-dimensional rectangular channel. Parametric studies showed that the effects of flow channeling and thermal dispersion are reduced significantly in three-dimensional configurations as compared with corresponding two-dimensional cases. Although this appears to be the first comprehensive study of three-dimensional forced convection in a porous duct, additional experimental and numerical studies are needed to analyze the important physical phenomena related to inertia effects, boundary effects, porosity variation and thermal dispersion in three-dimensional configurations of practical significance.

### References

Amiri, A. and Vafai, K. (1994), "Analysis of dispersion effects and non-thermal equilibrium, non-Darcian, variable porosity incompressible flow through porous media", *International Journal of Heat Mass Transfer,* Vol. 37, pp. 939-54.

Bartlett, R.F. and Viskanta, R. (1996), "Enhancement of forced convection in an asymmetrically heated duct filled with high thermal conductivity porous media", *Journal of Enhanced Heat Transfer,* Vol. 3, pp. 291-9.

Benenati, R.F. and Brosilow, C.B. (1962), "Void fraction distribution in beds of spheres", *AIChE Journal,* Vol. 8, pp. 359-61.

Chandrasekhara, B.C. and Vortmeyer, D. (1979), "Flow model for velocity distribution in fixed porous beds under isothermal conditions", *Thermal Fluid Dynamics,* Vol. 12, pp. 105-11.

Cheng, P., Hsu, C.T. and Chowdhury, A. (1988), "Forced convection in the entrance region of a packed channel with asymmetric heating", *ASME Journal of Heat Transfer,* Vol. 110, pp. 946-54.

Chou, F.C., Lien, W.Y. and Lin, S.H. (1992), "Analysis and experiment of non-Darcian convection in horizontal square packed-sphere channels – I. Forced convection", *International Journal of Heat Mass Transfer,* Vol. 35, pp. 195-205.

Ergun, S. (1952), "Fluid flow through packed columns", *Chemical Engineering Progresses,* Vol. 48, pp. 89-94.

Hsu, C.T. and Cheng, P. (1990), "Thermal dispersion in a porous medium", *International Journal of Heat Mass Transfer,* Vol. 33, pp. 1587-97.

Hunt, M.L. and Tien, C.L. (1988), "Effects of thermal dispersion on forced convection in fibrous media", *International Journal of Heat Mass Transfer,* Vol. 31, pp. 301-9.

Hwang, G.J. and Chao, C.H. (1994), "Heat transfer measurement and analysis for sintered porous channels", *ASME Journal of Heat Transfer,* Vol. 114, pp. 456-64.

Hwang, G.J. and Wu, C.C. (1995), "Drag and heat transfer measurement and analysis for porous channels", *ASME/JSME Thermal Engineering Conference,* Vol. 3, pp. 347-53.

Irvine Jr, T.F. (1963), "Non-circular duct convective heat transfer", *Modern Developments in Heat Transfer,* Academic Press, New York, NY, pp. 1-17.

Kaviany, M. (1995), *Principles of Heat Transfer in Porous Media,* Springer-Verlag, New York, NY.

Koch, D.L. and Brady, J.F. (1985), "The effective diffusivity of fibrous media", *AIChE Journal,* Vol. 32, pp. 575-91.

Kuzay, T.M., Collins, J.T. and Khounsary, A.M. (1991), "Enhanced heat transfer with metal-wool-filled tubes", *ASME/JSME Thermal Engineering Proceedings,* Vol. 5, pp. 451-9.

Nield, D.A. and Bejan, A. (1992), *Convection in Porous Media,* Springer-Verlag, New York, NY.

Patankar, S.V. (1980), *Numerical Heat Transfer and Fluid Flow,* Hemispheres, New York, NY.

Poulikakos, D. and Renken, K.J. (1987), "Forced convection in a channel filled with porous medium, including the effects of flow inertia, variable porosity, and Brinkman friction", *ASME Journal of Heat Transfer,* Vol. 109, pp. 880-8.

Renken, K.J. and Poulikakos, D. (1988), "Experiments on forced convection from a horizontal heated plate in a packed bed of glass spheres", *ASME Journal of Heat Transfer,* Vol. 111, pp. 59-65.

Shah, R.K. and London, A.L. (1978), "Laminar flow forced convection in ducts", *Advances in Heat Transfer,* suppl. 1, Academic Press, New York, NY.

Vafai, K. (1994), "Convective flow and heat transfer in variable porosity media", *Journal of Fluid Mechanics,* Vol. 147, pp. 233-59.

Vafai, K. and Tien, C.L. (1981), "Boundary and inertia effects on flow and heat transfer in porous media", *International Journal of Heat Mass Transfer,* Vol. 24, pp. 195-203.

Vafai, K., Alkire, R.L. and Tien, C.L. (1985), "An experimental investigation of heat transfer in variable porosity media", *ASME Journal of Heat Transfer,* Vol. 107, pp. 642-47.

Zehner, P. and Schluender, E.U. (1970), "Waermeleifahigkeit von schuettungen bei massingen temperaturen", *Chemical Engineering Technologies,* Vol. 42, pp. 933-41.